Journal of Non-Crystalline Solids: X 19 (2023) 100195

Contents lists available at ScienceDirect

Journal of Non-Crystalline Solids: X

journal homepage: www.sciencedirect.com/journal/journal-of-non-crystalline-solids-x

An overview on the effect of dissolved water on the viscosity of soda lime silicate melts

J. Deubener [a,*], H. Behrens [b], R. Müller [c]

[a] Institute of Non-Metallic Materials, Clausthal University of Technology, Clausthal-Zellerfeld 38678, Germany
[b] Institute of Mineralogy, Leibniz University of Hannover, Hannover 30167, Germany
[c] Bundesanstalt für Materialforschung und -Prüfung (BAM), Berlin 12489, Germany

ARTICLE INFO

Keywords:
Water in glass
Viscosity
Soda lime silicate glasses
Shear thinning
Hydrogen melting

ABSTRACT

In this review article, the impact of dissolved water on the viscous properties of soda lime silicate melts is addressed against the background of the upcoming switch from natural gas to hydrogen combustion. This change will lead to an increase in the total water content of the glasses by up to 0.4 mol%. In order to better define possible influences of water speciation, water-rich glasses were synthesised under increasing pressure up to the kbar range. It is shown that a distinction must be made between the influence of dissolved OH-groups and H_2O-molecules in order to accurately reflect the dependence of isokom temperatures on water content. In addition, an increase of one order of magnitude in the tolerance to higher deformation rates was observed for the range of expected increased water contents during isothermal deformation processes, which is based on the time-temperature superposition principle, i.e. congruent flow curves were determined under isokomal conditions.

1. Introduction

In the global glass industry, soda-lime silicate glasses have by far the largest production share (~70% of 150 million tonnes in 2014), which is divided between the container glass, flat glass and glass fibre sectors [1]. In all areas, thermomechanical melt properties play a crucial role, running like a thread from batch melting through shaping to cooling/reheating. Since in this system the main components are determined by the batch recipe, changes in the relevant properties can be caused by secondary components and traces whose contents vary due to the raw material quality and the parameters of the manufacturing technologies.

Special attention should be paid to the influence of dissolved water, which is directly related to the partial pressure of water vapour p_{H2O} in the melting tank. With the change from air-gas firing to oxygen-gas firing and nowadays to oxygen-hydrogen firing, p_{H2O} can reach 1 bar for stoichiometric combustion, which strongly increases the dissolved water content in the melt. Due to the molar mass difference between H_2O and an anhydrous ("dry") soda lime silicate glass (a factor of ~3), these water contents on a molar basis will correspond to the fractions of K_2O or Al_2O_3 in today's float glass formulations and will have technological and product-specific effects. For example, a change in the viscosity of the melt will be able to influence the entire manufacturing steps from melting to shaping and cooling, as water is a strong fluxing agent [2,3,4]. It should be noted that common terms such as "water dissolution" and "water enrichment" are used in this review in the context of manufacturing and that hydrous species are referred to as "OH-groups" and "H_2O-molecules" based on the assignment of the IR absorption spectrum, which greatly simplifies the complex mechanisms leading to hydrous silicate glasses and the actual species nature.

Another important aspect for industrial moulding is that several measurements have shown that soda lime silicate melts undergo viscous shear thinning at high strain rates [5,6], although silicate melts were long thought to exhibit pure Newtonian viscous flow, where the stress developed remains proportional to the strain rate. If the viscosity of hydrated melts decreases more at higher shear rates than anhydrous melts, it might be possible to use this property to speed up the processing rate without increasing the process temperature. On the other hand, water affects the redox state of multivalent ions, e.g. iron prefers the ferrous state when water is present [7,8]. Also, the water-sulphur interaction has to be considered [9]. Both can have superimposed effects on the workability of technical glass melts. Of course, the challenges associated with the conversion to hydrogen combustion in glass furnaces are more comprehensive - only the management of large amounts of water vapour in the tank and the expected faster corrosion of

* Corresponding author.
E-mail address: joachim.deubener@tu-clausthal.de (J. Deubener).

https://doi.org/10.1016/j.nocx.2023.100195
Received 31 March 2023; Received in revised form 14 June 2023; Accepted 20 June 2023
Available online 21 June 2023

the refractory material with the associated shorter service lives should be mentioned here. Strategies and techno-economic analyses for the introduction of hydrogen gas into oxyfuel glass melting are presented in [10,11] while the increase in water vapour content of the flue gas in the combustion space of the glass furnace is addressed in [12].

The objective of this topical review is to summarise the various facets of the influence of water enrichment in soda lime silicate melts on the technologically important flow properties, i.e. Newtonian and Non-Newtonian viscosity at temperatures above glass transition, which the authors have investigated on the same glass or very similar types of soda lime silicate glasses. This research, with its various aspects of water in glass, was based on the fundamental and inspiring work of Professor Minoru Tomozawa, who has shaped this area of glass research for decades like no other.

2. Parent glasses and water enrichment

The composition of technical soda lime silicate glasses can be derived from the archetypal composition 74–16–10 for SiO_2, Na_2O and CaO (mol %). In addition to this ternary base, up to 10 further components are present in small concentrations and traces in commercial soda lime silicate glasses, some of which originate from the raw material impurities or are added specifically for the various tasks in glass production and for the desired application-related property requirements. Since the focus here is on the minor component water, it is important to specify the different types of soda lime silicate glasses investigated, whose chemical compositions are shown in Table 1.

SLS, SLSa, FG and MSG glasses were enriched with water in a special procedure at the Institute of Mineralogy of Leibniz University Hannover. For this purpose, glass powders were enclosed in welded platinum capsules with certain amounts of water, remelted at temperatures above the liquidus temperature (1250–1400 °C) in an internally heated pressure vessel (IHPV) at pressures up to 500 MPa and quenched under pressure. Conditions were always water-undersaturated, i.e., no fluid bubbles remained in the glasses. IHPV syntheses resulted in water contents up to 21.5 mol%. Details of this synthesis route were presented in [16,18,19,17]. References glasses SCH [13], MER [2], MCM [14], SAK [3] and RAP [15] were enriched at ambient pressure by bubbling steam through the melt. Bubbling of steam through the melt (1450 °C) was also carried out at increased pressures up to 8 bar at the Federal Institute for Materials Research and Testing in Berlin.

After preparing hydrated glasses, the total water content was determined by Karl-Fischer-titration. In addition, NIR spectroscopy was used to distinguish between the contents of OH-groups and H_2O-molecules. For this purpose, the absorbance of the bands near to 5200 cm^{-1} (for H_2O-molecules) and 4500 cm^{-1} (for OH-groups) were evaluated. Details of the quantification procedure including the determination of the linear molar absorption coefficients can be found in [16,18] for SLS and FG glasses and in [17] for MSG glasses.

In addition to the chemical solubility of water in the form of OH-groups (water as a network modifier), there is also an increasing physical solubility of H_2O-molecules in the free volume of the glass network at higher p_{H2O} (water as a stuffing agent). Assume that an interconversion of OH-groups and H_2O-molecules takes place in the simplified form [20,21,22]:

$$H_2O + O = 2\ OH \tag{1}$$

where O stands for oxygen atoms of the anhydrous melt (charges are not considered), the equilibrium constant K of the interconversion reaction for an ideal mixing of these species is defined by

$$K = \frac{[OH]^2}{[H_2O][O]} \tag{2}$$

where molar fractions of the OH-, H_2O- and O-species are given in square brackets. For the temperature dependence of K,

$$lnK = \frac{\Delta S^0}{R} - \frac{\Delta H^0}{RT} \tag{3}$$

then applies, where R is the gas constant and ΔS^0, ΔH^0 are the standard state molar entropy or enthalpy of the interconversion reaction.

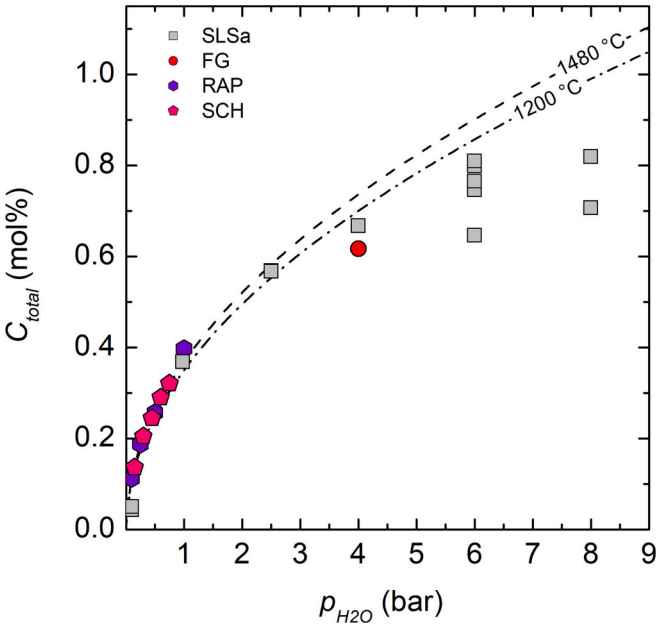

Fig. 1. Total water content C_{Total} as a function of the water vapour partial pressure during melting p_{H2O}. Data: SLSa and FG (unpublished), RAP [15] and SCH [20]. Lines are the water solubility in SCH glasses for steam bubbling according to $C_{Total} = L \times p_{H2O}^{0.5}$ with L = 0.35 mol% H_2O $bar^{-0.5}$ at 1200 °C and L = 0.368 mol% H_2O $bar^{-0.5}$ at 1480 °C [20].

Table 1
Analysed chemical composition (mol%) of the soda lime silicate starting glasses used for water enrichment experiments. See references for precision of the used analytic methods. Oxides in parentheses present a nominal molar amount < 0.05.

	SiO_2	Na_2O	CaO	MgO	Al_2O_3	K_2O	Fe_2O_3	TiO_2	B_2O_3	H_2O	Ref.
SCH	74.0	15.9	10.1							0.055	[13]
MER	75	15.0	10.0							0.013	[2]
MCM	73.8*	15.5*	10.7*							0.031	[14]
RAP	74*	16*	10*							0.112	[15]
SLS	73.4	15.5	10.1		(0+)	(0+)	(0+)			0.100	[16]
SLSa	74.1	15.8	10.2		(0+)	(0+)	(0+)			0.040	[16]
FG	71.4	12.6	9.5	5.8	0.4	0.2	(0+)			0.147	[16]
SAK	70.5	14.0	6.8	6.5	0.7	0.8			0.7	0.030	[3]
MSG	73.2	13.3	6.6	6.2	0.5	0.2	(0+)	(0+)		0.129	[17]

Key: *by batch.

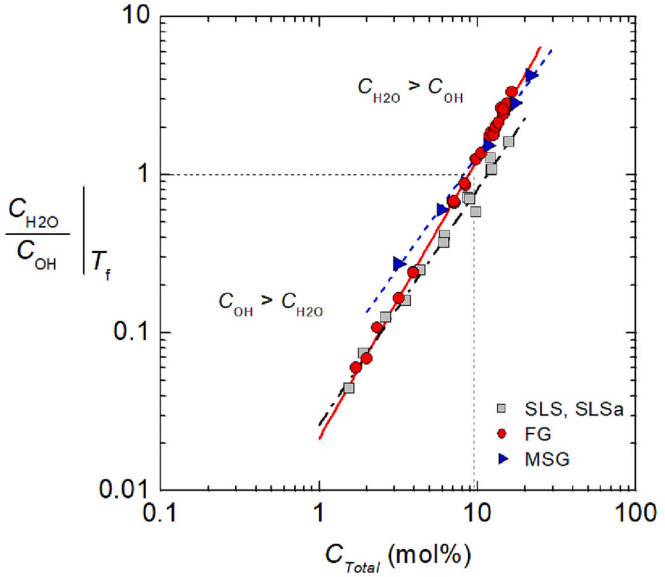

Fig. 2. C_{H2O}-to-C_{OH} ratio, frozen at the fictive temperature T_f, as a function of the total water content obtained from NIR spectroscopy. SLS data from [18,23], FG data from [18,19] and MSG data from [17]. Lines are the fit of Eq. (4) to the data.

3. Total water content and distribution into OH-groups and H_2O-molecules

Fig. 1 shows the water content obtained in mol% as a function of p_{H2O}. Reference measurements under ambient pressure by Scholze [20] and by Rapp and Shelby [15] were used for comparison. According to Eqs. (1) and (2), the equilibrium concentration of the water dissolved in these melts is a square root of the water vapour partial pressure during melting. For $p_{H2O} = 1$ bar, water contents of up to ~0.4 mol% can be achieved in soda lime silicate glasses, while no equilibrium solubility was reached for syntheses at $p_{H2O} > 3$ bar.

Fig. 2 shows the water speciation in hydrated soda lime silicate glasses, i.e. the ratio of the mol fractions of H_2O-molecules (C_{H2O}) to OH-groups (C_{OH}) was plotted as a function of the total water content C_{Total} ($= C_{H2O} + C_{OH}$). First, it can be seen that hydration under high p_{H2O} led to high total water contents up to 21.5 mol% in soda lime silica glasses. Furthermore, Fig. 2 clearly shows that water molecules dominate in hydrated glasses with a total water content larger than 8–11.5 mol%, while OH-groups predominate at lower total water contents. The dependence can be described by the following equation:

$$\frac{C_{H_2O}}{C_{OH}} = y\, C_{Total}{}^{n} \tag{4}$$

where y and n are adjustable parameters related to the interconversion reaction Eq. (2). Table 2 summarizes the values for y and n obtained by fitting Eq. (4) to the data of SLS, SLSa, FG and MSG data. For glasses melted at ambient pressure, this means that dissolved H_2O-molecules are negligible. Note that the determined C_{H2O}-to-C_{OH} ratio is a function of the glass transition temperature, i.e. the fictive temperature (T_f) of each composition at which the species concentrations are frozen under pressure during cooling. To obtain T_f data, the viscometric glass transition temperature T_{12} (T_{12} is the isokom temperature at which the viscosity takes the value 10^{12} Pa s) was used.

Fig. 3 shows that the temperature dependence of ln$K$ over $1/T$ is strongly negative for all three glasses according to Eq. (2), which means that OH-groups are strongly favoured with increasing temperature. As with the water speciation shown in Fig. 2, the dependence is somewhat steeper for hydrated FG glass than for MSG and SLS glasses. Furthermore, Fig. 3 shows that data with ln$K$ larger than −1.5 calculated from the C_{H2O}-to-C_{OH} ratio according to Eq. (3) deviate from the linear behaviour. This means that an extrapolation of the straight line in Fig. 2 only seems appropriate down to total water contents of ~0.2 mol% (MSG) to ~0.7 mol% (FG and SLS). At these C_{total} values, there is approximately one water molecule per one hundred OH-groups. The values of ΔS^0 and ΔH^0 obtained by fitting Eq. (3) to the data are summarised in Table 2. How T_{12} was extracted from the temperature dependence of viscosity is presented in the next chapter. It should be noted that T_{12} can deviate from the cooling conditions of the melts during hydration. In such a case, the affected data points would not represent the equilibrium conditions in the melt. For details of the cooling rates and relaxation of the glasses during water enrichment in the IHPV used, see [24,25].

4. Viscosity data of hydrous soda lime silicate melts

The viscosity of hydrated soda lime silicate melts was determined both near the glass transition temperature and above the liquidus temperature. For this purpose, viscometric methods were used at ambient pressure (micropenetration and parallel-plate [26,27]) and under 200–500 MPa (parallel-plate and falling sphere [19]). In the experiments under ambient pressure, water desorption from the surface of the sample is generally to be expected, so that the micropenetration measurement of SLSa, FG and MER glasses was usually conducted along a temperature-time protocol in which the change in viscosity between the start and end of the measurement was kept smaller than 0.1 log units. For parallel-plate viscometry at ambient pressure, the glass cylinders of SLSa and FG were relatively large (~10 mm diameter), so the effects of water desorption from the sample surface on viscosity are negligible.

Table 2
Parameters used for modelling the water speciation, the viscometric glass transition T_{12} and the melt fragility m of Eqs. (3), (4), (9) and (13), respectively. Numbers in parenthesis indicate the uncertainty of the last digit.

	Glass	FG	SLS, SLSa	MSG
	C_{total} (mol%)	1.7–16.4	1.5–15.7	3.1–21.5
Eq. (3)	ΔH^0 (kJ mol^{-1})	55.0(8)	32(2)	32(1)
	ΔS^0 (J mol^{-1} K^{-1})	57(1)	27(2)	25(2)
Eq. (4)	y	0.0214(7)	0.026(2)	0.051(6)
	n	1.77(1)	1.49(4)	1.42(5)
Eq. (9)	$T_{12(AG)}$ (K)	826(3)	837(9)	817(5)
	b (K)	0.14(3)	0.07(5)	0.15(2)
	c (K)	1.5(2)	1.7(4)	1.4(1)
	d (K)	−1.6(1)	−1.6(4)	−2.0(1)
Eq. (13)	m_{AG}	35.6(17)		35.1(21)
	b	0.1		0.06
	c	2.1		2.2
	d	−0.0001		−0.0002

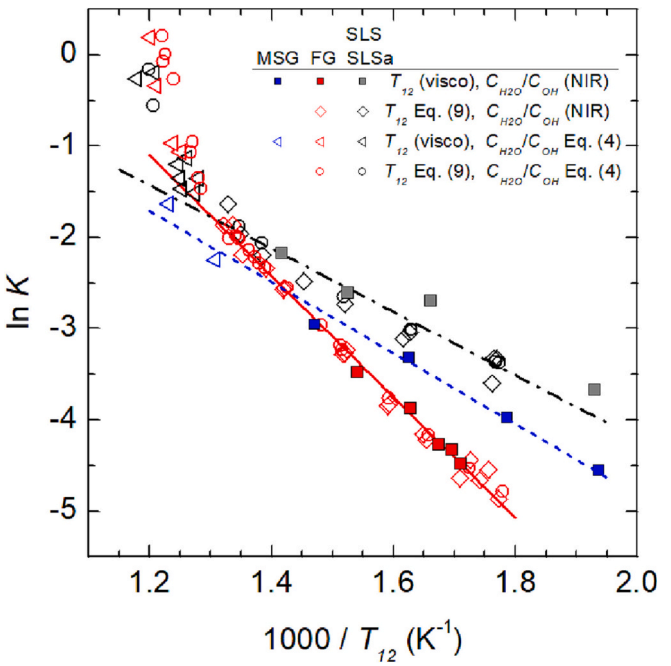

Fig. 3. Arrhenius diagram of the reaction constant K as a function of the viscometric glass transition temperature T_{12} assuming $T_{12} = T_f$. Lines are the fits of Eq. (3) to the data.

The same is true for parallel-plate tests of these glasses conducted under elevated pressure. Here, the sample size was much smaller, but due to the increased external pressure of 200–500 MPa, water desorption from the sample surface was not detectable. In addition, the pressure dependence of viscosity was found to be relatively small (the shift in T_{12} was 5 K per 100 MPa), so joint analysis of the data resulted in negligible error. For the description of the temperature-dependent viscosity, the MYEGA model in this overview was used [28]:

$$log\eta(T) = A + \frac{B}{T} exp\left(\frac{C}{T}\right) \tag{5}$$

where the adjustable parameters are the viscosity in the high temperature limit A (= log $\eta_{T\infty}$) and two constants B, C that are related to the onset of rigidity in the liquid network. The reformulation of Eq. (5) in terms of the viscometric glass transition temperature T_{12} and the kinetic fragility m of the melt leads to [28]:

$$log\eta = A + (12 - A)\frac{T_{12}}{T} exp\left[\left(\frac{m}{12 - A} - 1\right)\left(\frac{T_{12}}{T} - 1\right)\right] \tag{6}$$

while m can be expressed in the form:

$$m = (12 - A)\left[1 + ln\left(\frac{T_{12}}{B}(12 - A)\right)\right] \tag{7}$$

All data of previous studies were re-evaluated using Eq. (6) and shown in Fig. 4. In case no high temperature low viscosity data were available, $A = -3$ ($\eta_{T\infty} = 10^{-3}$ Pa s) was kept constant [28].

5. Modelling viscosity

Fig. 4 and Fig. 5 show that hydration of soda lime silicate glasses leads to a strong decrease in the viscometric glass transition temperature T_{12}, while the dependence of kinetic fragility m on total water content is less pronounced (Fig. 5). Hydration at ambient pressure (bubbling with steam) seems to lead to decreasing fragility values (MER, SAK and MCM reference glasses), but a clear trend cannot be established as the FG data are scattering. In order to perform such an analysis also for hydrous soda lime silicate glasses for which no viscosity data are available, the calorimetric glass transition temperature T_g was used instead of T_{12} assuming that the glass has experienced equal cooling and heating rates. Under this condition, T_g is equal with the fictive temperature T_f, i.e. the glass is free of thermal history and the characteristic temperature of the onset of the endothermic DSC signal (tangent construction [29]) through the glass transition interval is:

$$log\eta(T_g) = K_{T_{onset}} - logq \tag{8}$$

for the viscosity η in the unit Pa s, the cooling/heating rate q in the units K s^{-1} and the shift factor $K_{Tonset} = 11.2 \pm 0.15$ [30,31,29]. Thus, for $q =$ 0.167 K s^{-1} (10 K min^{-1}) one obtains log $\eta = 12 \pm 0.15$. The strong dependence of T_{12} on total water content has been used to model the viscosity of hydrated glasses. Tomozawa [4], who introduced a three-component model in which the contributions of OH-groups and H_2O-molecules to the T_{12} decay are weighted, pioneered this work. Later, the contributions of the water species were normalised to a water content (0.02 wt%) common in industrial production [32], while Schneider et al. [33] added a quadratic term to the original model to better describe the asymmetric T_{12} composition curve. His equation in the following form was used to analyse the T_{12} dependence on the total water content C_{total} (mol%) [33]:

$$\begin{aligned} T_{12}(C_{Total}) = {} & w_1 T_{12(H2O)} + w_2 T_{12(AG)} + c w_1 w_2 \left(T_{12(AG)} - T_{12(H2O)}\right) \\ & + d w_1 w_2{}^2 \left(T_{12(AG)} - T_{12(H2O)}\right) \end{aligned} \tag{9}$$

with

$$w_1 = \frac{C_{Total}}{b(100 - C_{Total}) + C_{Total}} \text{ and } w_2 = \frac{b(100 - C_{Total})}{b(100 - C_{Total}) + C_{Total}}, \tag{10}$$

where the adjustable parameters are b, c and d and the glass transition of the anhydrous glass $T_{12(AG)}$. The glass transition of water $T_{12(H2O)}$ is 136 K [34]. The curves in part (A) of Fig. 5 show that for the entire range of water contents the T_{12} fits of Eq. (9) to the FG, SLSa and MSG data are in very good agreement with the experimental values. The parameters of these fits are given in Table 2.

To introduce the change in melt fragility into the modelling of hydrous soda lime silicate glasses, the approximation of Langhammer et al. [36] was first used, who assumed that the rigidity parameter B of the MYEGA model is independent of C_{total}. Then, Eq. (7) has the form [36]:

$$m = m_{AG} + (12 - A)\, ln\left(\frac{T_{12}}{T_{12(AG)}}\right) \tag{11}$$

where m_{AG} and $T_{12(AG)}$ are the fragility and the viscometric glass transition of the anhydrous melt, respectively. A consequence of this simplification is that the viscosity of hydrated soda lime silicate melts depends only on T_{12} when $T_{12(AG)}$ is specified. It also predicts a progressive decrease in m as T_{12} drops sharply with C_{Total} (Fig. 5).

As elastic constants for hydrous MSG glasses were determined by ultrasonic echography [17], m was also modelled by the ratio between shear modulus and bulk modulus. Cassetta et al. [37] found that melt fragility and Pugh's modulus k (defined as the ratio between shear modulus and bulk modulus to distinguish the ductile/brittle behaviour of polycrystalline materials [38] and metallic glasses [39]) in volcanic silicate melts are inversely related in the form [37]:

$$m = \frac{43}{k} - 31 \tag{12}$$

Although the validity of a linear relationship between melt fragility and inverse Pugh's modulus across different classes (inorganic, organic, metallic) of glassy materials has been questioned (see, e.g., [40,41,42]), this approach is used here because in the analysis of Cassetta et al. [37], in addition to volcanic melts, some technologically relevant silicate melts were also used for the calibration of Eq. (12), in particular the soda lime standard glass DGG-1. Fig. 5 shows that the application of Eq. (12)

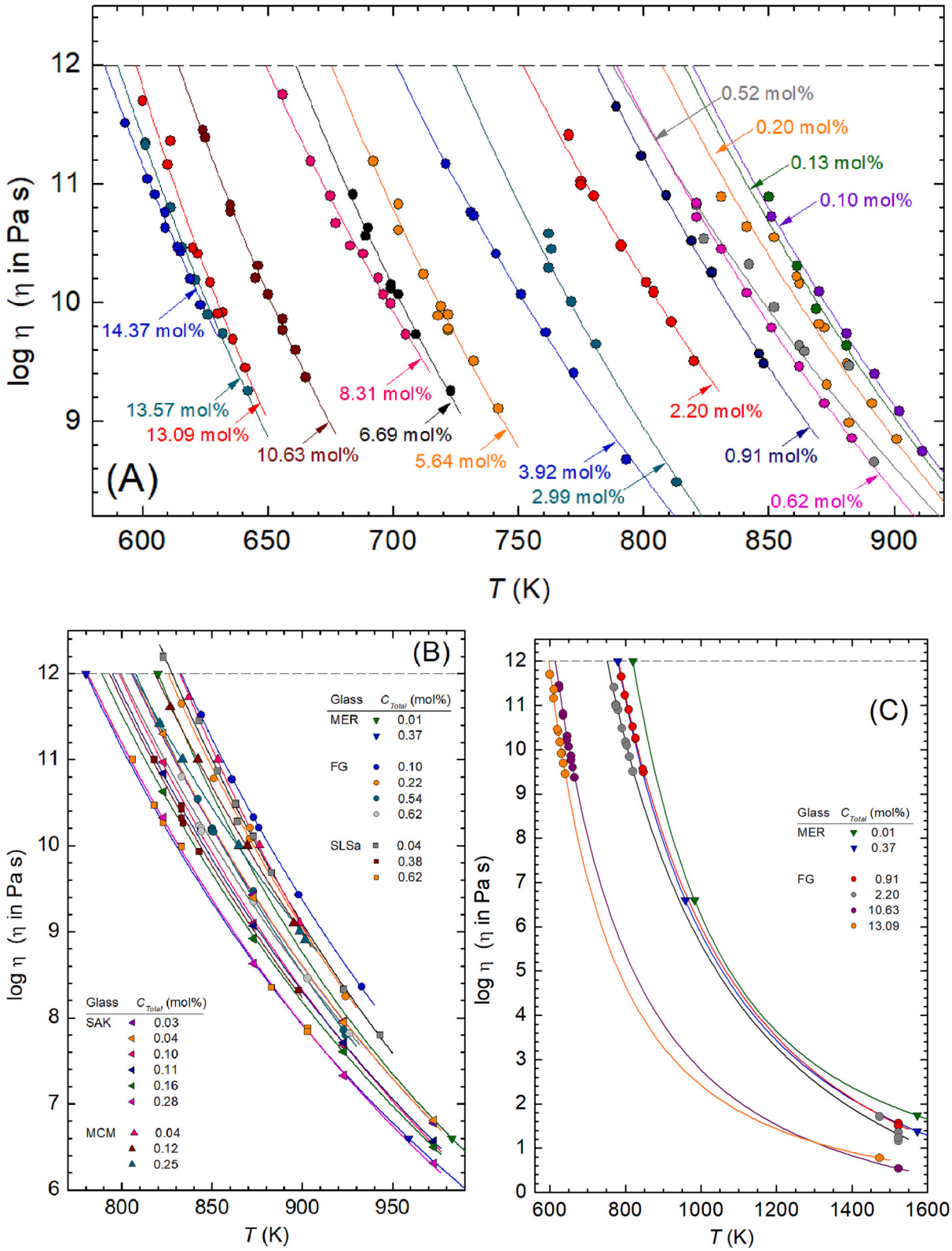

Fig. 4. Viscosity of hydrous soda lime silicate melts as a function of temperature. Part (A) shows viscosities obtained at 200 MPa for FG glasses prepared in an IHPV [19], while part (B) shows viscosity data of MER, FG, SLSa, SAK and MCM glasses (hydrated in water vapour) from [2], [26], [14] obtained at ambient pressure. Part (C) shows data of MER and FG glasses from [2,19] where low and high viscosities were determined. Lines in all part are the fits of Eq. (6) to the data.

to the hydrous MSG glasses leads first to a decreasing and then (> 3 mol %) to an increasing melt fragility with increasing water content. This would imply that water in form of OH-groups has an opposite effect on the thermal resistivity of the melt structure than dissolved water molecules, which is in line with opposite effects reported for volumetric [13],[14],[17] and elastic properties [14] of the corresponding glasses at room temperature. Note that setting $A = -3$ for those melts for which no high-temperature data are available increasingly underestimates the

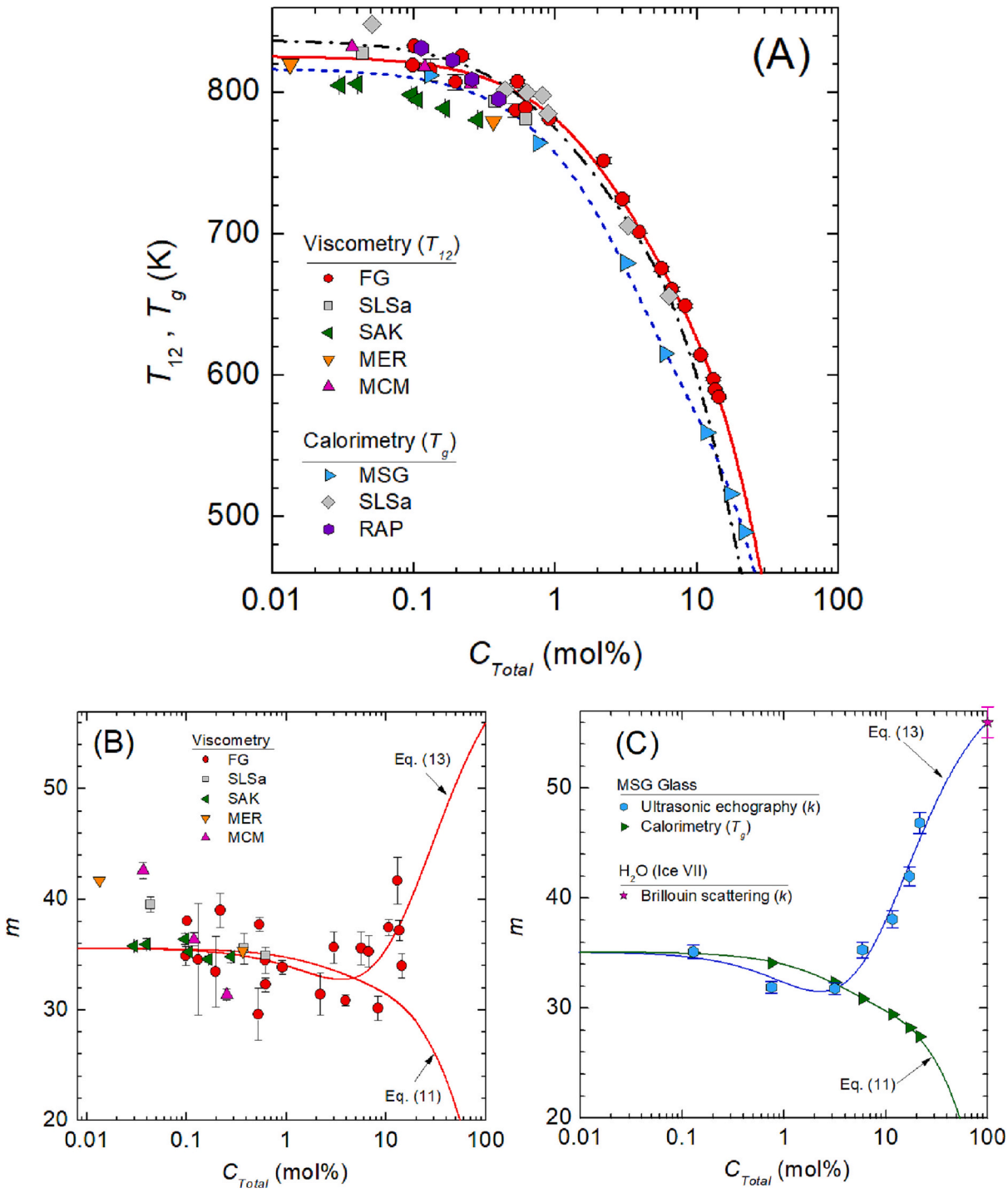

Fig. 5. Viscometric T_{12} and calorimetric T_g glass transition as a function of the total water content C_{Total} (A). Kinetic fragility m obtained directly from viscometry (B) and indirectly from Pugh's modulus and T_g data for the MSG glass [17] (C). Lines in part (A) are the fits of Eq. (9) to the FG (continuous red line), SLSa (black dashed dotted line) and MSG (blue dotted line) data. Lines in parts (B) and (C) are the fits of Eq. (11) and Eq. (13) to the FG and MSG data, respectively. Pugh's modulus k of ice VII from [35]. (For interpretation of the references to colour in this figure legend, the reader is referred to the web version of this article.)

fragility index as the water content of the melt increases. The opposite effect of OH-groups and H_2O-molecules on m in Fig. 5 is in turn supported by the FG melts with reliable high-temperature data (falling sphere tests under elevated pressure of 200–500 MPa in order to minimize water losses). To include this more complex behaviour into the modelling, we assume that the three-component model Eq. (9) can also be used to describe the asymmetric composition dependence of the melt fragility. Therefore, the fragility of the end-member water was calculated using Pugh's modulus of ice VII, which is $k = 0.502$ at 10 GPa and 0.487 at 40 GPa [39]. Note that in hydrous silicate glasses the occupied volume resembles that of densest molecular form of H_2O, that is, ice VII [40,41,42]. Then, using Eq. (12) for the hypothetical melt fragility of water one has $m_{H2O} = 56 \pm 1.4$ and the modified Eq. (9) has the form:

$$m(C_{Total}) = w_1 m_{H2O} + w_2 m_{AG} + c w_1 w_2 (m_{AG} - m_{H2O}) + d w_1 w_2^2 (m_{AG} - m_{H2O}) \quad (13)$$

The parameters of the fits of Eq. (13) to the FG and MSG data are given in Table 2.

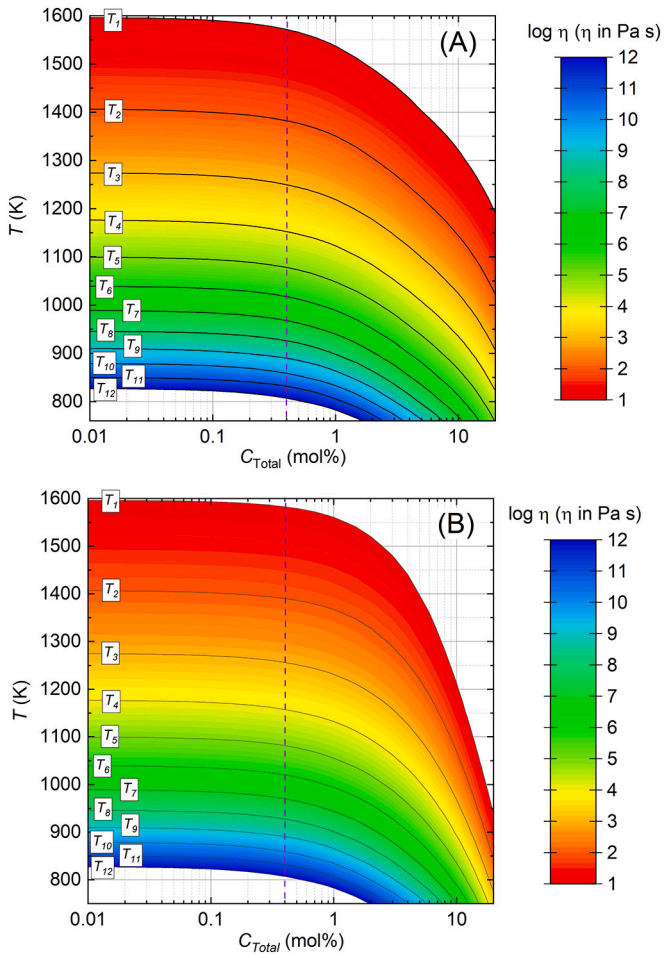

Fig. 6. Modelled viscosity of FG melts as a function of the total water content (mol%) and temperature (K). Isokom temperatures are given by continuous black lines. Vertical dashed line indicate water solubility for $p_{H2O} = 1$ bar. Part (A) assumes melt fragility according to Eq. (11) while part (B) melt fragility is modelled according to Eq. (13).

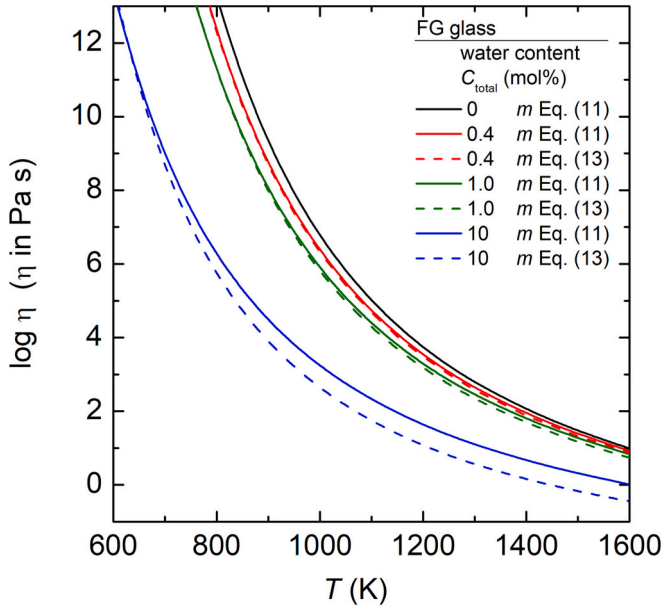

Fig. 7. Modelled viscosity of FG melts as a function of temperature for a total water content $C_{Total} = 0$, 0.4, 1 and 10 mol%.

To model the melt viscosity for all temperatures and water contents, the parameters of Eq. (9) listed in Table 2 were used to determine T_{12} and Eq. (11) to determine m for the calculated T_{12}. Alternatively, Eq. (13) was used to determine m for the calculated T_{12}. The two contour plots of Fig. 6 show exemplary results for hydrous FG glass melts (For the anhydrous melt, one has $m_{AG} = 35.6$ if $A = -3$ is kept constant in Eq. (11)). The FG type was used here as it most closely matches the composition of technical soda lime silicate glasses and has the highest data density. Fig. 6 shows that the ambiguity regarding the fragility of high water content melts has little effect on the isokom temperatures of melts enriched with water vapour under ambient pressure. To exemplify this in the usual way, Fig. 7 shows the viscosity (log units) as a function of temperature for a selected total water content $C_{Total} = 0$, 0.4, 1 and 10 mol%. The first total water content (0) represents the anhydrous melt, the second (0.4) refers to the water solubility at $p_{H2O} = 1$ bar, while the third (1) and fourth total water content (10) were selected to illustrate the effect of the different trend of m with increasing water content (see Fig. 5B) on the temperature-dependent viscosity.

6. Shear rate dependence

In addition to determining Newtonian viscosity, parallel plate compression of glass cylinders was carried out at high piston speeds up to 0.2 m s^{-1}. Force deformation data were recorded with high time resolution and the data were mechanically and thermally corrected for load frame stiffness and energy dissipation during cylinder compression. Details of this method are described in [43]. Fig. 8 shows sections of **Fig. 4**B for FG and SLSa glasses. The isokomal ($T_{10.2}$ and $T_{10.28}$) and isothermal (844 K and 823 K) conditions were selected for high-speed deformation tests [24].

The onset of shear thinning was measured at deformation rates $\dot{\varepsilon}$ of 10^{-4} to 10^{-3} s^{-1}, which was five log units above the deformation rate at which Newtonian viscosity was determined (Fig. 9). Finally, the process of shear thinning at higher deformation rates was experimentally limited by melt fracturing. Shear thinning was described by the Yue-Brückner flow equation in terms of the ratio between apparent and Newtonian viscosity [44]:

$$\frac{\eta}{\eta_0} = \frac{\eta_\infty}{\eta_0} + \left(1 - \frac{\eta_\infty}{\eta_0}\right)\left(1 - exp\left(-\frac{\dot{\varepsilon}}{\dot{\varepsilon}_g}\right)\right)\frac{\dot{\varepsilon}_g}{\dot{\varepsilon}} \quad (14)$$

where η is the rate dependent (apparent) viscosity, η_0, η_∞ are rate independent viscosities for $\dot{\varepsilon}\to 0$ and $\dot{\varepsilon}\to\infty$ respectively, $\dot{\varepsilon}$ is the deformation rate and is the $\dot{\varepsilon}_g$ flow relaxation rate. The parameters of the fits of Eq. (14) to the FG and SLSa data were compiled in Table 3.

Fig. 9 shows that for isothermal deformation processes, the onset of shear thinning in the water-enriched melts shifts to higher rates by about one order of magnitude. The effect seems to be somewhat more pronounced with the Mg- and Al-free SLSa melt than for the Mg- and Al-containing FG melt. In contrast, the comparison based on equal Newtonian viscosities (Fig. 10) shows that the shift in the flow curves in Fig. 9 is largely due to the decrease in isokom temperature in accordance with the time-temperature superposition principle [45]. All flow curves thus almost overlap when comparing the low-water parent melt with the more water-rich melts at lower temperatures, resulting in the same Newtonian viscosity. It can therefore be stated within the investigated C_{total} range that the isokomal workability of soda lime silicate melts is practically independent of the water content. This is in agreement with the expected trend as the melt fragility is only marginally affected by the water content between 0.04 and 0.62 mol%. Note that Newtonian flow is considered as a steady-state response of the relaxed structure to the applied stress, while a nonlinear effect at high deformation rates reflects the incomplete relaxation of the melt and the orientation of the structural units [46]. In particular, the rate-dependent viscosity and onset of shear thinning are reported to be controlled by the melt configuration, e.

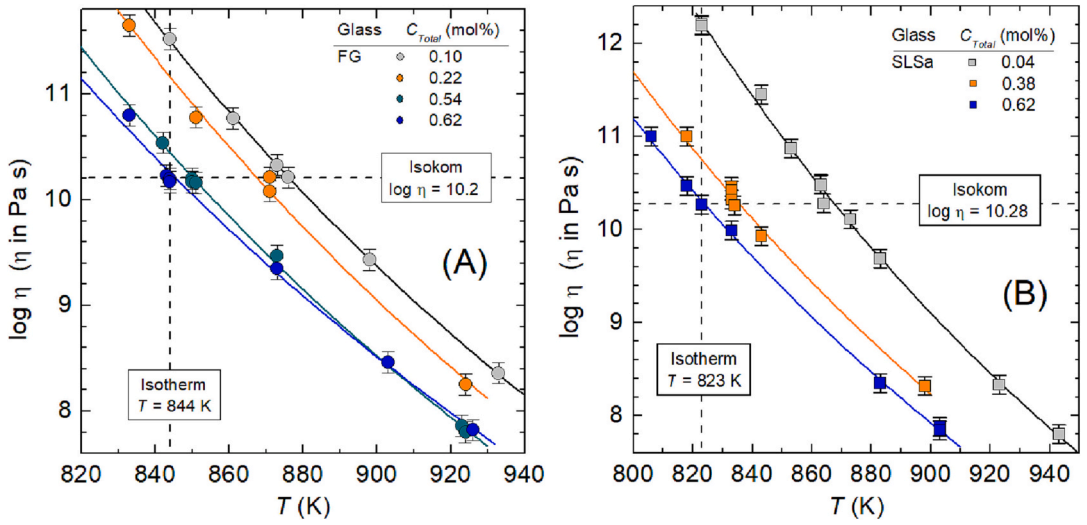

Fig. 8. Selection of isothermal and isokomal conditions for high-speed deformation tests of hydrous soda lime silicate glasses. FG and SLSa data from [24]. Lines in all part are the fits of Eq. (6) to the data.

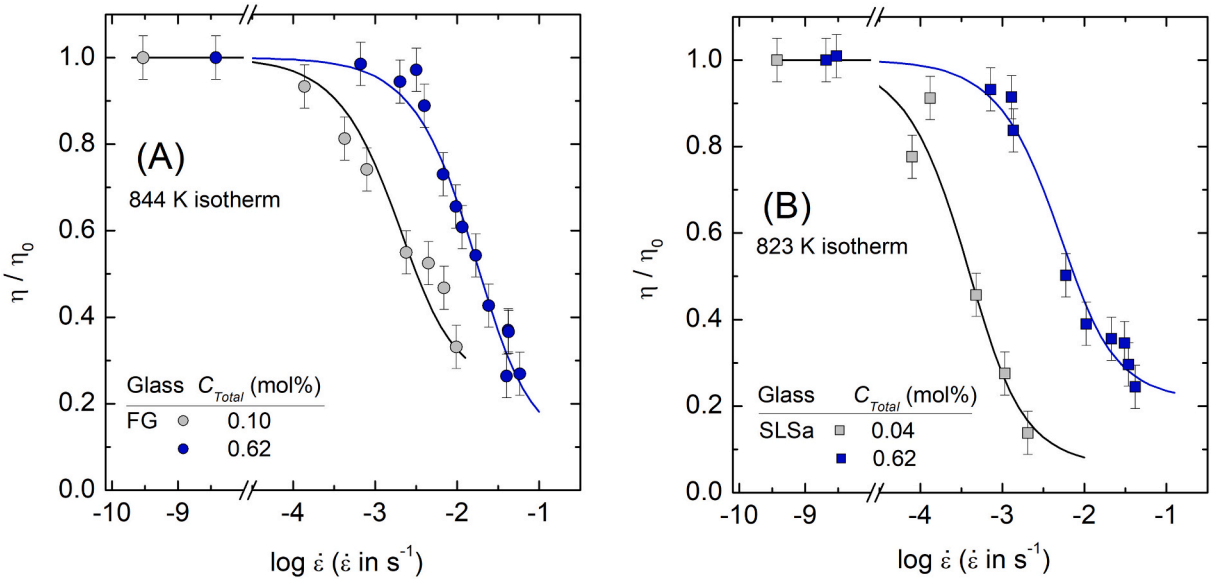

Fig. 9. Apparent viscosity normalised to Newtonian viscosity as a function of the deformation rate of the parent glass and a water-enriched FG glass (A) and SLSa glass (B) under isothermal conditions. The lines are the fit of Eq. (14) to the data. FG and SLSa data from [24].

Table 3
Non-Newtonian flow parameters η_∞/η_0 and log $\dot{\varepsilon}_g$of Eq. (14) of hydrous FG and SLSa glasses under isokomal and isothermal conditions.

Glass	C_{Total} (mol%)	Isokomal condition			Isothermal condition		
		$T_{10.2}$ (K)	η_∞/η_0 (%)	log $\dot{\varepsilon}_g$ ($\dot{\varepsilon}_g$ in s^{-1})	T (K)	η_∞/η_0 (%)	log $\dot{\varepsilon}_g$ ($\dot{\varepsilon}_g$ in s^{-1})
FG	0.10	876	23.4	−2.13	844	23.2	−2.92
	0.22	871	30.1	−2.60			
	0.54	850	32.1	−2.44			
	0.62	844	8.9	−1.99	844	8.9	−1.99
		$T_{10.28}$ (K)	η_∞/η_0 (%)	log $\dot{\varepsilon}_g$ ($\dot{\varepsilon}_g$ in s^{-1})	T (K)	η_∞/η_0 (%)	log $\dot{\varepsilon}_g$ ($\dot{\varepsilon}_g$ in s^{-1})
SLSa	0.04	864	12.5	−2.21	823	5.9	−3.64
	0.38	834	27.1	−2.83			
	0.62	823	21.2	−2.52	823	21.2	−2.52

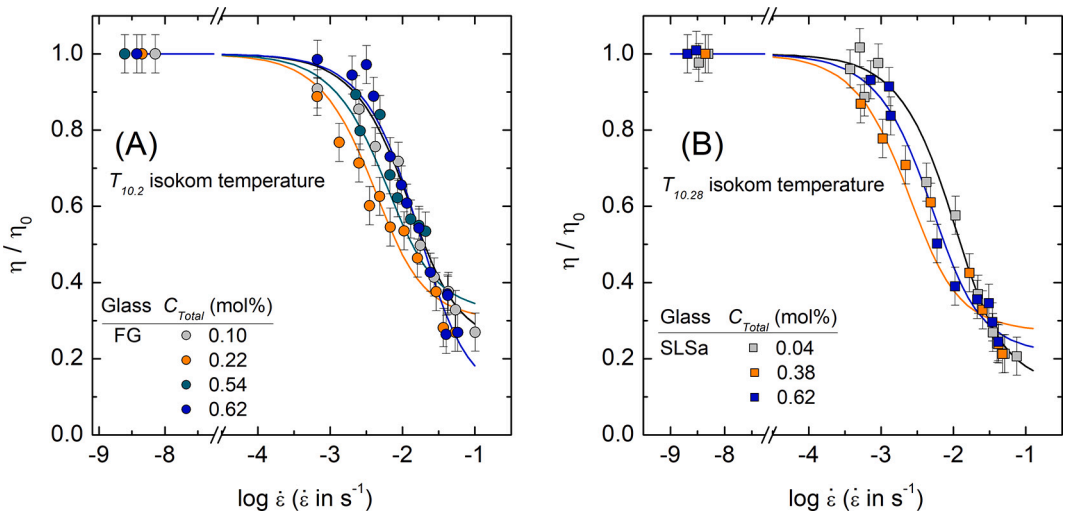

Fig. 10. Apparent viscosity normalised to Newtonian viscosity as a function of the deformation rate of the parent glass and water-enriched FG glasses (A) and SLSa glasses (B) under isokomal conditions. The lines are the fit of Eq. (14) to the data. FG and SLSa data from [24].

g. the degree of polymerisation, as shown by comparing synthetic meta- and disilicate compositions with industrial flat glasses [47].

7. Summary

An increased water vapour partial pressure, as can be expected with hydrogen-oxygen firing, leads to an increased water content in soda lime silicate glasses, which can reach 0.4 mol% at 1 bar. Under these conditions, the species ratio of dissolved H_2O-molecules to OH-groups is still very low (about 1:100). The network modifying character of the chemically dissolved water therefore determines the viscosity of the melt. For the industrial relevant FG glass, this leads to a decrease in the T_{12} isokom temperature of about 14.4 K for an increase in C_{Total} from 0.1 to 0.4 mol%. The resistance to thermal depolymerisation is only slightly weakened in the C_{Total} range 0.1–0.4 mol%, as almost all species are already present as OH-groups at the glass transition, i.e. the melt fragility decreases only marginally. At higher water contents, the experimental results unfortunately show a strong scattering in the fragility values, and indirect determinations via the calorimetric glass transition temperature and the ratio of shear to compression modulus of the corresponding glasses lead to opposite trends. With respect to the equilibrium constant of the interconversion reaction between OH-groups and H_2O-molecules, the modifying property should be more prominent for the high temperature range, as H_2O-molecules will convert to OH-groups, which could stop or even reverse the decreasing trend of m with C_{total}. Despite the uncertainty of m at higher water contents reserved for high-pressure processes, the viscosity behaviour could be fully modelled with the approaches presented here for all industrially accessible water contents and temperatures. Furthermore, workability analysis testing of water-enriched melts under high-speed deformation, shows about an order of magnitude higher tolerance to shear thinning and melt fracture on an isotemperature basis, largely due to the lowering of the isokom temperature of the Newtonian viscosity.

CRediT authorship contribution statement

J. Deubener: Conceptualization, Methodology, Validation, Formal analysis, Visualization, Writing – original draft, Writing – review & editing. **H. Behrens:** Conceptualization, Methodology, Validation, Formal analysis, Visualization, Writing – original draft, Writing – review & editing. **R. Müller:** Conceptualization, Methodology, Validation, Formal analysis, Visualization, Writing – original draft, Writing – review & editing.

Declaration of Competing Interest

The authors declare that they have no known competing financial interests or personal relationships that could have appeared to influence the work reported in this paper.

Data availability

Data will be made available on request.

Acknowledgments

We gratefully acknowledge support of the Deutsche Forschungsgemeinschaft (DFG) by grants Be 1720/9, De 598/4, Mu 963/4 in 2001–2006 and by the priority program SPP 1594 in 2012–2020. In particular, we thank the former PhD students R. Balzer, P. del Gaudio, P. Kiefer, A. Stuke, T. Waurischk and S. Zietka for their work on hydrous soda lime silicate glasses and melts.

References

[1] C.D. Westbroek, J. Bitting, M. Craglia, J.M.C. Azevedo, J.M. Cullen, Global material flow analysis of glass: from raw materials to end of life, J. Ind. Ecol. 25 (2021) 333–343.
[2] L. Merker, H. Scholze, Der Einfluß des Wassergehaltes von Silikatgläsern auf ihr Transformations- und Erweichungsverhalten, Glastech. Ber. 35 (1962) 37–43.
[3] S. Sakka, K. Matusita, T. Watanabe, K. Kamiya, Effects of small amounts of water on the viscosity, glass transition temperature and hardness of silicate glasses, J. Jap. Ceram. Soc. 89 (1981) 578–584.
[4] M. Tomozawa, M. Takata, J. Acocella, E.B. Watson, T. Takamori, Thermal properties of $Na_2O{\cdot}3SiO_2$ glasses with high water content, J. Non-Cryst. Solids 56 (1983) 343–348.
[5] R. Brückner, New results in the glass forming under extreme conditions, in: A. K. Varshneya, D.E. Bickford, P.P. Bihuniak (Eds.), Advances in Fusion and Processing of Glass, Ceram, Trans, vol. 29, The American Ceramic Society, Westerville, 1993, pp. 3–24.
[6] J.H. Simmons, T.P. Swiler, C.J. Simmons, Studies of nonlinear vicous flow in silicate glasses, in: A.K. Varshneya, D.E. Bickford, P.P. Bihuniak (Eds.), Advances in Fusion and Processing of Glass, Ceram, Trans, vol. 29, The American Ceramic Society, Westerville, 1993, pp. 3–24.
[7] R. Brückner, H. Hessenkemper, Influence of water content and basicity on redox ratio – consequences on radiation, heat absorption and emission of glass melts during fusion and processing, Glastech. Ber. 66 (1993) 245–253.
[8] R. Brückner, Y. Yue, Isothermal and isochomal workability of glass melts – influence of melting history: minor composition changes of redox state and hydroxyl content – a study of the sensitivity of the cylinder compression method, Glastech. Ber. Glas. Sci. Technol. 69 (1996) 348–356.
[9] M. Vernerová, J. Kloužek, L. Němec, Reaction of soda–lime–silica glass melt with water vapour at melting temperatures, J. Non-Cryst. Solids 416 (2015) 21–30.

[10] S. Gärtner, D. Rank, M. Heberl, M. Gaderer, B. Dawoud, A. Haumer, M. Sterner, Simulation and techno-economic analysis of a power-to-hydrogen process for oxyfuel glass melting, Energies 14 (2021) 8603.
[11] H.P.H. Muijsenberg, H. Mahrenholtz, Carbon reduction comparison of electric or hydrogen power, in: S.K. Sundaram (Ed.), 82nd Conf. On Glass Problems, Ceram. Transact vol. 270, Wiley, 2022, pp. 117–137.
[12] M. Adendorff, R.L. Bell, S. Chakravarti, H. Kobayashi, M. Shah, Preparing for sustainable glass production – Technical and economic investigation of next generation fuels for glass melters, in: S.K. Sundaram (Ed.), 82nd Conf. On Glass Problems, Ceram. Transact vol. 270, Wiley, 2022, pp. 139–152.
[10] H. Scholze, H. Franz, L. Merker, Der Einbau des Wassers in Gläsern, VI: Der Einfluß des Wassers auf einige Glaseigenschaften, insbesondere Dichte und Lichtbrechung, Glastechn. Ber. 32 (1959) 421–426.
[11] P.W. McMillan, A. Chlebik, The effect of hydroxyl ion content on the mechanical and other properties of soda-lime-silica glass, J. Non-Cryst. Solids 38 & 39 (1980) 509–514.
[12] D.B. Rapp, J.E. Shelby, Water diffusion and solubility in soda–lime–silica melts, Phys. Chem. Glasses 44 (2003) 393–400.
[13] H. Behrens, A. Stuke, Quantification of H_2O contents in silicate glasses using IR spectroscopy - a calibration based on hydrous glasses analyzed by Karl-Fischer titration, Glas. Sci. Technol. 76 (2003) 176–189.
[14] P. Kiefer, R. Balzer, J. Deubener, H. Behrens, T. Waurischk, S. Reinsch, R. Müller, Density, elastic constants and indentation hardness of hydrous soda-lime-silica glasses, J. Non-Cryst. Solids 521 (2019), 119480.
[15] A. Stuke, H. Behrens, B.C. Schmidt, R. Dupree, H_2O speciation in float glass and soda lime glass, Chem. Geol. 229 (2006) 64–77.
[16] P. del Gaudio, H. Behrens, J. Deubener, Viscosity and glass transition temperature of hydrous float glass, J. Non-Cryst. Solids 353 (2007) 223–236.
[17] H. Scholze, Der Einbau des Wassers in Gläsern, II. UR-Messungen an Silikatgläsern mit systematisch variierter Zusammensetzung und Deutung der OH-Banden in Silikatgläsern, Glastechn. Ber. 32 (1959) 142–152.
[18] R.F. Bartholomew, B.L. Butler, H.L. Hoover, C.K. Wu, J. Am, Ceram. Soc. 63 (1980) 481–485.
[19] E. Stolper, The speziation of water in silicate melts, Geochim. Cosmochim. Acta 46 (1982) 2609–2620.
[20] S. Reinsch, R. Müller, J. Deubener, H. Behrens, Internal friction of hydrated soda-lime-silicate glasses, J. Chem. Phys. 139 (2013), 174506.
[21] H. Behrens, M. Nowak, Quantification of H_2O speciation in silicate glasses and melts by IR spectroscopy – in situ versus quench techniques, Phase Transit. 76 (2003) 45–61.
[22] H. Behrens, Water speciation in oxide glasses and melts, Chem. Geol. 558 (2020), 119850.
[23] J. Deubener, H. Behrens, R. Müller, S. Zietka, S. Reinsch, Kinetic fragility of hydrous soda-lime-silica glasses, J. Non-Cryst. Solids 354 (2008) 4713–4718.
[24] S. Zietka, Newton'sche und nicht Newton'sche Viskosität wasserhaltiger Silicatschmelzen, Dissertation,, TU Clausthal, 2019.
[25] J.C. Mauro, Y. Yue, A.J. Ellison, P.K. Gupta, D.C. Allan, Viscosity of glass-forming liquids, Proc. Natl. Acad. Sci. U. S. A. 106 (2009) 19780–19784.
[26] D. Di Genova, A. Zandona, J. Deubener, Unravelling the effect of nano-heterogeneity on the viscosity of silicate melts: implications for glass manufacturing and volcanic eruptions, J. Non-Cryst. Solids 545 (2020), 120248.
[27] G.W. Scherer, Use of the Adam-Gibbs equation in the analysis of structural relaxation, J. Am. Ceram. Soc. 67 (1984) 504–511.
[28] Y.Z. Yue, R. Von der Ohe, S.L. Jensen, Fictive temperature, cooling rate, and viscosity of glasses, J. Chem. Phys. 120 (2004) 8053–8059.
[29] J. Deubener, R. Müller, H. Behrens, G. Heide, Water and the glass transition temperature of silicate melts, J. Non-Cryst. Solids 330 (2003) 268–273.
[30] H.A. Schneider, J. Rieger, E. Penzel, The glass transition temperature of random copolymers: 2. Extension of the Gordon Taylor equation for asymmetric Tg vs composition curves, Polymer 38 (1997) 1323–1337.
[31] I. Kohl, L. Bachmann, E. Mayer, A. Hallbrucker, T. Loerting, Glass transition in hyperquenched water? Nature 435 (2005) E1.
[32] D. Langhammer, D. Di Genova, G. Steinle-Neumann, Modelling the viscosity of anhydrous and hydrous volcanic melt, Geochem. Geophys. Geosyst. 22 (2021) e2021GC009918.
[33] M. Cassetta, D. Di Genova, M. Zanatta, T. Boffa Ballaran, A. Kurnosov, M. Giarola, G. Mariotto, Estimating the viscosity of volcanic melts from the vibrational properties of their parental glasses, Sci. Rep. 11 (2021) 13072.
[34] S.F. Pugh XCII, Relations between the elastic moduli and the plastic properties of polycrystalline pure metals, Philos. Mag. 7 (1954) 823–843.
[35] J.J. Lewandowski, W.H. Wang, A.L. Greer, Intrinsic plasticity or brittleness of metallic glasses, Philos. Mag. Lett. 85 (2005) 77–87.
[36] V.N. Novikov, A.P. Sokolov, Poisson's ratio and the fragility of glass-forming liquids, Nature 431 (2004) 961–963.
[37] S.N. Yannopoulos, G.P. Johari, Glass behaviour: Poisson's ratio and liquid's fragility, Nature 442 (2006) 961–963.
[38] A.P. Sokolov, V.N. Novikov, A. Kisliuk, Fragility and mechanical moduli: do they really correlate? Philos. Mag. 87 (2007) 613–621.
[39] W. Shi, N. Sun, X. Li, Z. Mao, J. Liu, V.B. Prakapenka, Single-crystal elasticity of highpressure ice up to 98 GPa by Brillouin scattering, Geophys. Res. Lett. 48 (2021) e2021GL092514.
[40] P. Richet, A. Polian, Water as a dense icelike component in silicate glasses, Nature 281 (1998) 396–398.
[41] P. Richet, A. Whittington, F. Holtz, H. Behrens, S. Ohlhorst, M. Wilke, Water and the density of silicate glasses, Contrib. Mineral. Petrol. 138 (2000) 337–347.
[42] A. Whittington, P. Richet, A. Polian, Water and the compressibility of silicate glasses: a Brillouin spectroscopic study, Am. Mineral. 97 (2012) 455–467.
[43] R. Brückner, Y. Yue, A. Habeck, Determination of the reological properties of high-viscous glass melts by the cylinder compression method, Glastech. Ber. 67 (1994) 114–129.
[44] Y. Yue, R. Brückner, A new description and interpretation of the flow behaviour of glass forming melts, J. Non-Cryst. Solids 180 (1994) 66–79.
[45] M.A. Bohn, The connection between the parameters of WLF equation and of Arrhenius equation, Propellants Explos. Pyrotech. 44 (2019) 696–705.
[46] R. Brückner, About the origin of non-Newtonian flow of glass melts, Glastech. Ber. Glas. Sci. Technol. 67C (1994) 161–166.
[47] Y. Yue, R. Brückner, Comparison of some non-Newtonian flow equations for inorganic glass melts and amorphous polymers, J. Non-Cryst. Solids 202 (1996) 253–265.